



1 **Contrasting effects of secondary organic aerosol formations on organic aerosol**
2 **hygroscopicity**

3 **Ye Kuang^{1,2}, Shan Huang^{1,2*}, Biao Xue^{1,2}, Biao Luo^{1,2}, Qicong Song^{1,2}, Wei Chen³, Weiwei Hu³,**
4 **Wei Li^{1,2}, Pusheng Zhao⁴, Mingfu Cai^{1,2}, Yuwen Peng^{1,2}, Jipeng Qi^{1,2}, Tiange Li^{1,2}, Duohong**
5 **Chen⁵, Dingli Yue⁵, Bin Yuan^{1,2}, Min Shao^{1,2*}**

6 ¹ Institute for Environmental and Climate Research, Jinan University, Guangzhou, China.

7 ² Guangdong-Hongkong-Macau Joint Laboratory of Collaborative Innovation for Environmental
8 Quality, Guangzhou, China.

9 ³ State Key Laboratory of Organic Geochemistry and Guangdong Key Laboratory of Environmental
10 Protection and Resources Utilization, Guangzhou Institute of Geochemistry, Chinese Academy of
11 Sciences, Guangzhou 510640, China

12 ⁴ Institute of Urban Meteorology, China Meteorological Administration, Beijing 100089, China

13 ⁵ Guangdong Ecological and Environmental Monitoring Center, State Environmental Protection Key
14 Laboratory of Regional Air Quality Monitoring, Guangzhou 510308, China

15 *Correspondence to: Shan Huang (shanhuang_eci@jnu.edu.cn) and Min Shao (mshao@pku.edu.cn)

16

17 **Abstract**

18 Water uptake abilities of organic aerosol under sub-saturated conditions play critical roles in direct
19 aerosol radiative effects and atmospheric chemistry, however, field characterizations of organic aerosol
20 hygroscopicity parameter κ_{OA} under sub-saturated conditions remain limited. In this study, a field
21 campaign was conducted to characterize κ_{OA} at relative humidity of 80% with hourly time resolution
22 for the first time in the Pearl River Delta region of China. Observation results show that during this
23 campaign secondary organic aerosol (SOA) dominated total organic aerosol mass (mass fraction >70%
24 on average), which provides us a unique opportunity to investigate influences of SOA formation on
25 κ_{OA} . Results demonstrate that the commonly used organic aerosol oxidation level parameter O/C was
26 weakly correlated with κ_{OA} and failed in describing the variations of κ_{OA} . However, the variations
27 in κ_{OA} were well reproduced by mass fractions of organic aerosol factor resolved based on aerosol
28 mass spectrometer measurements. The more oxygenated organic aerosol (MOOA) factor, exhibiting
29 the highest average O/C (~1) among all organic aerosol factors, was the most important factor driving
30 the increase of κ_{OA} and was commonly associated with regional air masses. The less oxygenated



31 organic aerosol (LOOA, average O/C of 0.72) factor, revealed strong daytime production, exerting
32 negative effects on κ_{OA} . Surprisingly, the aged biomass burning organic aerosol (aBBOA) factor also
33 formed quickly during daytime and shared a similar diurnal pattern with LOOA, but had much lower
34 O/C (0.39) and had positive effects on κ_{OA} . The correlation coefficient between κ_{OA} and mass
35 fractions of aBBOA and MOOA in total organic aerosol mass reached above 0.8. The contrasting
36 effects of LOOA and aBBOA formation on κ_{OA} demonstrates that volatile organic compound (VOC)
37 precursors from diverse sources and different SOA formation processes may result in SOA with
38 different chemical composition, functional properties as well as microphysical structure, consequently,
39 exert distinct influences on κ_{OA} and render single oxidation level parameters (such as O/C) unable to
40 capture those differences. Aside from that, distinct effects of aBBOA on κ_{OA} was observed during
41 different episodes, suggesting that the hygroscopicity of SOA associated with similar sources might
42 also differ much under different emission and atmospheric conditions. Overall, these results highlight
43 that it is imperative to conduct more researches on κ_{OA} characterization under different
44 meteorological and source conditions, and examine its relationship with VOC precursor profiles and
45 formation pathways to formulate a better characterization and develop more appropriate
46 parameterization approaches in chemical and climate models.

47
48

49 **1 Introduction**

50 Organic aerosol (OA) composed of hundreds to thousands of organic species is one of the
51 dominant aerosol components in the atmosphere and exert significant effects on climate and
52 environment (Jimenez et al., 2009). The water uptake ability of atmospheric organic aerosol plays key
53 roles in aerosol direct radiative effects and aerosol-cloud interactions (Rastak et al., 2017; Liu and
54 Wang, 2010), and also aerosol liquid water content (Li et al., 2019; Jin et al., 2020) thus atmospheric
55 chemistry. However, the hygroscopicity parameter κ_{OA} that describes the water uptake abilities of
56 organic aerosol remains poorly quantified and mechanisms behind κ_{OA} variations are not well
57 understood (Kuang et al., 2020b). Atmospheric OA is usually composed of both primary or secondary
58 organic aerosol components. Primary OA (POA) is directly emitted from anthropogenic and natural
59 sources such as biomass burning, coal and fossil fuel combustion, cooking and biogenic emissions.



60 Whereas secondary OA (SOA) is typically formed through atmospheric oxidation of volatile organic
61 compounds (VOCs) or aging processes of POA. It is commonly thought that OA becomes more
62 oxidized during its evolution in the atmosphere and will in general be more hygroscopic after aging
63 processes (Jimenez et al., 2009). A few studies have investigated the relationship between κ_{OA} and
64 aerosol oxidation state parameters such as O/C ratio or f44 (fraction of m/z 44 in OA measurements of
65 aerosol mass spectrometers). Some results, especially those from laboratory studies, demonstrated that
66 κ_{OA} was highly correlated with O/C (Jimenez et al., 2009; Massoli et al., 2010; Kuang et al.,
67 2020a; Zhao et al., 2016; Lambe et al., 2011), however, other researches demonstrated that κ_{OA} was
68 not or only weakly correlated with O/C (Cerully et al., 2015; Latham et al., 2013; Yeung et al.,
69 2014; Alfarra et al., 2013). As the research continues, it was revealed that many factors can have
70 significant impacts on κ_{OA} , such as different functional groups, carbon chain length and aerosol liquid
71 water content, etc. (Rickards et al., 2013; Suda et al., 2014; Petters et al., 2017; Marsh et al., 2017; Liu
72 et al., 2018). Kuang et al. (2020b) recently reviewed laboratory and field measurements of κ_{OA} and
73 concluded that O/C is not enough in parameterizing κ_{OA} and that additional parameters are needed.
74 Therefore, it is worthwhile and imperative to endeavor on κ_{OA} quantifications and parametrizations,
75 especially, considering that organic aerosol might play more critical roles in atmospheric environment
76 and climate for decades to come under strict control on anthropogenic emissions.

77 Most previous studies on κ_{OA} focused on laboratory studies, usually investigating κ_{OA} of SOA
78 produced from laboratory chamber systems, which might be far different from real atmospheric SOA
79 spectral. Quantifications of κ_{OA} based on field measurements remain relatively limited and are also
80 urgently needed to yield complementary information, which in turn might provide guidance for the
81 design of future laboratory studies. It is important to conduct more researches on κ_{OA} spatiotemporal
82 distributions and examine its relationship with OA profiles to reach a better characterization and give
83 rise to more appropriate parameterization approaches in chemical and climate models. China is a
84 country that has been experiencing severe aerosol pollution and has been undergoing rapid changes
85 under drastic air pollution control measures. However, despite the importance of organic aerosol
86 hygroscopicity, only few studies attempted to quantify κ_{OA} based on field measurements (Wu et al.,
87 2016; Li et al., 2019; Hong et al., 2018; Gunthe et al., 2011), mainly focusing on the North China Plain
88 (NCP). The Pearl River Delta (PRD) region is much cleaner than the NCP in terms of particulate matter
89 pollution, suggesting that distinct regions in China are at different stages of air pollution controls (Xu



90 et al., 2020). The composition of PM_{2.5} (particulate matter with aerodynamic diameter less than 2.5
91 μm) also differs much among regions, for example, OA and SOA fractions are much higher in the PRD
92 than those in the NCP and their precursors are also much different (Zhou et al., 2020a). More
93 investigations on κ_{OA} based on field studies in regions other than the NCP are urgently required.

94 In addition, most field studies on κ_{OA} only gave an estimate of the average κ_{OA} (Gunthe et
95 al., 2011) or an average statistical relationship between κ_{OA} and O/C (Wu et al., 2013) and only few
96 studies have reported κ_{OA} of higher time resolution featuring its diurnal variation characteristics
97 (Deng et al., 2019), and almost no studies have reported κ_{OA} with high time resolution. Kuang et al.
98 (2020a) proposed a new method to estimate κ_{OA} based on aerosol optical hygroscopicity
99 measurements and bulk aerosol chemical composition measurements, which yielded κ_{OA} estimates
100 at hourly time resolution. Based on this dataset, it was found that variations in κ_{OA} were highly
101 correlated with mass fractions of oxygenated organic aerosol in OA. In this study, the same method
102 was applied to the dataset acquired from field measurements at a background site of the PRD region.
103 High time resolution characterization of κ_{OA} and aerosol chemical properties were also achieved,
104 which enabled us to dig deeper on what factors other than O/C drove the variations of κ_{OA} and to
105 further elucidate on the complexity and possible approaches in parameterizing κ_{OA} based on field
106 measurements. Details on aerosol measurements and the κ_{OA} estimation method were presented in
107 Sect.2 and Sect.3, respectively. An overview of campaign data and general factors driving aerosol
108 chemistry was presented in Sect 4.1. The variations in estimated κ_{OA} and its relationship to OA
109 oxidation state and to distinct OA factors were presented and discussed in Sect 4.2. The complexity
110 regarding κ_{OA} was further demonstrated and elucidated in Sect 4.3.

111 **2 Measurements**

112 **2.1 Sampling site**

113 Physical, optical and chemical properties of ambient aerosol particles as well as meteorological
114 parameters and gas pollutants such as CO, O₃ and NO_x were continuously measured during autumn
115 (from 30th September to 17th November 2018) at a rural site in Heshan county, Guangdong province,
116 China. This site locates at a small mountain (22°42'N, 112°55'E, altitude of 55 m), about 55 km away
117 from megacity Guangzhou and is surrounded by villages and small residential towns and thus is little
118 influenced by local industrial sources. The location of this site is also shown in Fig.S1.



119 2.2 Aerosol physical properties measurements

120 During this field campaign, instruments were placed in an air-conditioned room. Two inlets were
121 housed on the roof of the three-floors building for aerosol sampling and both inlets are about 1.8 m
122 above the floor. One of the inlets was a PM₁₀ impactor with a 1.8 m long Nafion drier that lowers the
123 sample RH down to less than 30% placed downstream of it. A flow splitter was placed below the drier
124 and instruments downstream of this splitter include an Aerodynamic Particle Sizer (APS, TSI Inc.,
125 Model 3321, flow rate of 5 L/min), which measured the size distribution of ambient aerosol particles
126 of aerodynamic diameter about 600 nm to 20 μm; an AE33 aethalometer (Drinovec et al., 2015) with
127 a flow rate of 5 L/min, which measures aerosol absorption coefficients at seven wavelengths; a
128 humidified nephelometer system with a flow rate of about 6 L/min. The total flow rate of these
129 instruments was about 16 L/min, which was quite close to the flow rate of 16.7 L/min required by the
130 PM₁₀ impactor. Thus, these instruments measured physical and optical properties of PM₁₀ particles.

131 The humidified nephelometer system is a laboratory self-assembled one, including two Aurora
132 3000 nephelometers. One nephelometer measures aerosol scattering properties (scattering and back
133 scattering coefficients at three wavelengths: 450 nm, 525 nm, 635 nm) at a reference RH (called dry
134 Nephelometer because of sampling RH is lower than 30%), and another nephelometer measures
135 aerosol scattering properties under a fixed RH of 80% (called wet Nephelometer and the actual
136 sampling RH fluctuates within ±1%). Details on the humidifier and control algorithm can be found
137 in Kuang et al. (2020a). Note that to make sure the accuracy of the measured RH in the sensing volume
138 of the wet Nephelometer, three Vaisala HMP110 sensors with accuracies of ±0.2 °C and ±1.7 %
139 for RH between 0 to 90% were used to monitor the RH at different parts of the wet nephelometer. Two
140 were placed at the inlet and outlet of the wet nephelometer, one was placed in the sensing volume. The
141 water vapor pressure calculated from these three sensors must be strictly consistent with each other
142 (relative difference between any two of the sensors must be less than 2 %). Then the sampling RH of
143 the wet nephelometer was calculated using the averaged water vapor pressure and the sample
144 temperature measured by the sensor placed in the sensing volume of the wet nephelometer.

145 Another inlet was connected with a PM_{2.5} impactor (BGI SCC2.354, cut diameter of 2.5 μm with
146 flow rate of 8 L/min) and was also equipped with a Nafion drier lowering sampling RH down to less
147 than 30%. Downstream of this inlet were a soot particle aerosol mass spectrometer (SP-AMS,



148 Aerodyne Research, Inc., Billerica, MA, USA) and a scanning mobility particle sizer (SMPS; TSI
149 model 3080), which measured particle number size distribution (PNSD) ranging from 10 nm to 760
150 nm.

151 **2.3 SP-AMS measurements and data analysis**

152 The SP-AMS was deployed to measure size-resolved chemical composition for submicron
153 aerosol particles. The SP-AMS is basically a high-resolution time-of-flight aerosol mass spectrometer
154 (HR-ToF-AMS) combining a laser vaporization device, i.e., soot particle (SP) mode. The instrument
155 principle has been provided in previous papers (Canagaratna et al., 2007; Onasch et al., 2012). In brief,
156 HR-ToF-AMS containing a tungsten vaporizer can provide information of those particulate species
157 vaporized under around 600°C. By adding a Nd:YAG (1064nm) laser module inside of the HR-ToF-
158 AMS, the vaporizing temperature can increase to around 4000°C, enabling the SP-AMS to detect
159 refractory compositions such as black carbon (BC) and metals. After vaporized, the gaseous
160 components are ionized in electron impact (70eV) way and then quantitatively measured by a time-of-
161 flight mass spectrometer. Controlled by the orifice as well as aerodynamic lens of SP-AMS, particles
162 with diameter in submicrometer range are measured. During the Heshan Campaign, SP-AMS was
163 located next to a SMPS to minimize the sampling discrepancy. The SP-AMS alternately switched
164 between the V-mode (only tungsten vaporizer) and SP-mode (laser and tungsten vaporizer). The
165 original time resolution of SP-AMS data was 1 min (per run), and 15min average values were used in
166 this study to avoid disturbance from mode switching. During the campaign, the calibration system for
167 SP-AMS was not available and we used the values of ionization efficiency (IE) and relative ionization
168 efficiency (RIE) of different species from the latest successful calibration. The applied RIEs for default
169 SP-AMS species are: 1.1 for nitrate, 4 for ammonium, 1.2 for sulfate, 1.4 for organics and 1.3 for
170 chloride. The composition dependent collection efficiency (CDCE) was applied to mentioned species
171 following the instruction of Middlebrook et al.(2012). Refractory BC from SP-AMS was calculated
172 by mass concentration of family C_x ions from high resolution mass spectrometer times a scaling factor
173 (8) derived by comparison with equivalent BC mass concentration from AE33. SP-AMS data
174 evaluation was performed by specific software Squirrel (v1.61) for unit mass resolution and Pika
175 (v1.21) for high resolution based on Igor Pro (v6.37, WaveMetrics, Inc., Oregon, USA). Aside from



176 the good consistency between the aerosol from derived from SMPS and SP-AMS components as
177 mentioned in Sect.3.2, the resulting mass concentrations from SP-AMS were further validated by
178 consistency with the results from external measurements in the same site, e.g., filter measurements and
179 online measurements using gas aerosol collection system (GAC) with ion chromatography. More
180 details of SP-AMS data quality assurance will be provided in a parallel paper (Huang et al., in
181 preparation).

182 The source apportionment of organic aerosols (OA) was performed by positive matrix
183 factorization (PMF) based on high resolution OA data collected in V-mode (only tungsten vaporizer).
184 As a widely used source analysis method, PMF has been described in previous papers (Paatero,
185 1997;Paatero and Tapper, 1994). PMF using AMS data can be conducted by an Igor Pro-based panel,
186 i.e., PMF Evaluation Tool (PET, v2.06, Ulbrich et al., 2009). We input the matrices for OA mass
187 concentration and uncertainty into the model and operated it according to the instruction in Ulbrich et
188 al. (Ulbrich et al., 2009). Isotopes and ions with $m/z > 120$ were excluded to minimize the interference
189 from repeatedly calculated uncertainties and noise signals. In total, 454 ions were considered in PMF.
190 After investigating different solutions with factor number from 2 to 10, a six-factor solution was chosen
191 based on the best performance shown by PMF quality parameters and most reasonable source
192 identification. Two primary OA factors were identified including a hydrocarbon-like OA (HOA,
193 containing cooking emissions) and a biomass burning OA (BBOA). The other four factors were related
194 to secondary formation or ageing process: 1) more oxygenated OA (MOOA, regional transport), 2)
195 less oxygenated OA (LOOA, related to daytime photochemical formation), 3) nighttime-formed OA
196 (Night-OA), and 4) aged BBOA (aBBOA). The mass spectral profile and time series of OA factors
197 were shown in Figure S3, and OA factors with identified sources will be discussed in Set. 4. More
198 details on PMF solution selection and source identification will be provided in a parallel paper (Huang
199 et al., in preparation).

200

201 **3 Methodology**

202 **3.1 Aerosol hygroscopicity derivation from aerosol light scattering measurements**

203 The aerosol light scattering enhancement factor $f(RH, \lambda) = \frac{\sigma_{sp}(RH, \lambda)}{\sigma_{sp}(dry, \lambda)}$, $\sigma_{sp}(RH, \lambda)$ is the



204 aerosol scattering coefficient at light wavelength of λ and condition of RH, and was only measured
205 at 80% RH. Thus the aerosol hygroscopicity parameter $\kappa_{f(\text{RH})}$ was derived from $f(80\%, 525 \text{ nm})$.
206 The principle of this method is to find a diameter independent hygroscopicity parameter κ that fits the
207 observed $f(80\%, 525 \text{ nm})$ best. Although Kuang et al. (2017) proposed a simple method for
208 deriving $\kappa_{f(\text{RH})}$ based only on measurements of the humidified nephelometer system, in this study,
209 the more traditional method described therein was adopted to retrieve $\kappa_{f(\text{RH})}$, which uses
210 measurements of PNSD as inputs of Mie theory and the κ -Köhler theory. The idea of deriving $\kappa_{f(\text{RH})}$
211 from aerosol light scattering measurements was first proposed by Chen et al. (2014), however, the
212 physical understanding of $\kappa_{f(\text{RH})}$ was not mathematically interpreted until the study of Kuang et al.
213 (2020a). Briefly, $\kappa_{f(\text{RH})}$ can be approximately understood as the overall hygroscopicity of aerosol
214 particles with aerosol scattering coefficient contribution as the weighting function for size-resolved κ
215 distribution. Results of Kuang et al. (2020a) demonstrated that for typical continental aerosols $\kappa_{f(\text{RH})}$
216 represents the overall hygroscopicity of aerosol particles with a dry diameter range between 200 and
217 800 nm, thus no matter if $\kappa_{f(\text{RH})}$ values were retrieved based on aerosol light scattering enhancement
218 factor measurements downstream of a PM_{10} or a PM_1 impactor, they are almost the same, which was
219 confirmed by direct measurements in Kuang et al. (2020a) (observed average relative difference about
220 3.5%).

221 **3.2 Organic aerosol hygroscopicity derivation based on aerosol chemical composition and optical** 222 **hygroscopicity measurements**

223 Aerosol hygroscopicity parameter κ were usually calculated using measured aerosol chemical
224 composition based on volume mixing rule (κ_{chem}) to represent the aerosol hygroscopicity of aerosol
225 particles of certain diameters or present the overall hygroscopicity of the entire aerosol populations of
226 PM_1 . In this study, the size-resolved aerosol chemical compositions of PM_1 were measured using the
227 SP-AMS, however, the overall aerosol hygroscopicity was only derived based on aerosol light
228 scattering measurements of PM_{10} bulk aerosols. Results of (Kuang et al., 2020a) demonstrated that
229 κ_{chem} calculated based on bulk chemical compositions of PM_1 are quite consistent with $\kappa_{f(\text{RH})}$ of
230 PM_1 therefore also consistent with $\kappa_{f(\text{RH})}$ of PM_{10} . We have simulated the $\kappa_{f(\text{RH})}$ of PM_{10} and
231 κ_{chem} of PM_1 under different PNSDs coupled with different size-resolved κ distribution scenarios, as



232 shown in Fig.S2a. As shown in the results in Fig.S2b, $\kappa_{f(\text{RH})}$ of PM_{10} and κ_{chem} of PM_1 are quite
233 close to each other and the simulated average relative difference ($\frac{\kappa_{f(\text{RH}),\text{PM}_{10}} - \kappa_{chem,\text{PM}_1}}{\kappa_{chem,\text{PM}_1}} \times 100\%$) was -
234 $0.4 \pm 3\%$. Thus, $\kappa_{f(\text{RH})}$ of PM_{10} was used as the measured κ_{chem} in the following discussions.

235 The SP-AMS measures size-resolved PM_1 mass concentrations of SO_4^{2-} , NO_3^- , NH_4^+ , Cl^- and
236 organic aerosol, thus provides their bulk mass concentrations. A simplified ion pairing scheme was
237 used to derive mass concentrations of different inorganic salts (as listed in Tab.1) based on measured
238 bulk ion mass concentrations (Gysel et al., 2007; Wu et al., 2016). Note that the hygroscopicity
239 parameter was measured at RH of 80%, the κ values of ammonium sulfate and ammonium nitrate at
240 80% RH were predicted using the Extended Aerosol Inorganic Model (E-AIM), whose predictions for
241 ammonium nitrate and ammonium sulfate has been proven to be consistent with laboratory results
242 (Luo et al., 2020; Jing et al., 2018), and those of potassium chloride and ammonium bisulfate were
243 consistent with Liu et al. (2014)

244 **Table 1.** Densities (ρ) and hygroscopicity parameters (κ) of inorganic salts used in this study

Species	NH_4NO_3	NH_4HSO_4	$(\text{NH}_4)_2\text{SO}_4$	KCl
	(AN)	(ABS)	(AS)	(PC)
ρ (g cm^{-3})	1.72	1.78	1.769	1.98
κ	0.56	0.56	0.56	0.89

245 Note that Cl^- was coupled with K^+ due to that biomass burning events prevailed during this field
246 campaign. The simple volume mixing rule called Zdanovskii–Stokes–Robinson (ZSR) was usually
247 used for κ_{chem} calculations, that is, bulk κ_{chem} of PM_1 can be calculated on the basis of volume
248 fractions of different compounds (ε_i) (Petters and Kreidenweis, 2007) using the following equation:

$$249 \kappa_{chem} = \sum_i \kappa_i \cdot \varepsilon_i \quad (1)$$

250 And κ_i and ε_i are hygroscopicity parameter κ and volume fraction of compound i in the mixture.
251 Based on Eq.2 and Tab,1, κ_{chem} can be formulated as follows:

$$252 \kappa_{chem} = \kappa_{AS}\varepsilon_{AS} + \kappa_{AN}\varepsilon_{AN} + \kappa_{ABS}\varepsilon_{ABS} + \kappa_{PC}\varepsilon_{PC} + \kappa_{BC}\varepsilon_{BC} + \kappa_{OA}\varepsilon_{OA} + \kappa_X\varepsilon_X \quad (2)$$

253 where κ_{OA} and ε_{OA} are κ and volume fraction of entire organic aerosol populations, κ_X and ε_X are
254 κ and volume fraction of aerosol constituents which are beyond the detection ability of the SP-AMS.
255 The hygroscopicity of these unidentified aerosol species, in continental regions, likely be dust but still



256 possible composed of other components such as biogenic primary aerosol, were not discussed before.
257 On the basis of current literature reports, dust is nearly hydrophilic and varies a lot, with κ of mineral
258 dust and road dust as well as oil or coal fly ash are in the range of 0.01 to 0.08 (Koehler et al., 2009; Peng
259 et al., 2020). In this paper, κ_X is arbitrarily specified as 0.05. The ε_X are estimated as the PM₁
260 volume concentration difference between measured by the SMPS and calculated from volume
261 concentration summation of chemical compounds listed in Tab.1 and volume concentrations of BC
262 and organic aerosol, and the estimated average contribution ε_X during this campaign is 13% as shown
263 in Fig.S4. In the volume concentration calculations of BC and organic aerosol, BC density of 1.7 g/cm³
264 was assumed, and organic aerosol density is calculated based on the density parameterization scheme
265 proposed by Kuwata et al. (2012) using the organic aerosol elemental ratios O:C and H:C measured
266 by the SP-AMS as input parameters. In addition, κ_{BC} was set to zero due to the hydrophilic property
267 of BC particles. Then, κ_{OA} can be estimated based on measured κ_{chem} using the following formula:

$$268 \quad \kappa_{OA} = \frac{\kappa_{chem} - (\kappa_{AS}\varepsilon_{AS} + \kappa_{AN}\varepsilon_{AN} + \kappa_{ABS}\varepsilon_{ABS} + \kappa_{PC}\varepsilon_{PC} + \kappa_X\varepsilon_X)}{\varepsilon_{OA}} \quad (3)$$

269 **4 Results and discussions**

270 **4.1 Overview of the campaign data**

271 The time series of meteorological parameters such as wind speed, wind direction, RH and ambient
272 air temperature, aerosol scattering coefficients, aerosol hygroscopicity parameter $\kappa_{f(RH)}$, mass
273 concentrations of aerosol components as well as gas pollutant concentrations are shown in Fig.1.
274 During this campaign, the RH mainly ranged from 50% to 80% with an average ($\pm 1\sigma$) of $60 \pm 14\%$,
275 with the nighttime RH frequently reached beyond 70%, which favors the nighttime aqueous phase
276 chemistry. Temperatures mainly ranged from 18 to 28 °C, with an average ($\pm 1\sigma$) of 23.6 ± 3.3 °C,
277 indicating a relatively warm state during this campaign though in the autumn. The aerosol scattering
278 coefficients at 525 nm ($\sigma_{sp,525}$) shown in Fig.1b demonstrate $\sigma_{sp,525}$ generally ranged between 20 to
279 600 Mm^{-1} , with an average ($\pm 1\sigma$) of $256 \pm 102 \text{ Mm}^{-1}$, indicating moderately polluted conditions during
280 this campaign. The NR-PM₁ mass concentrations ranged from 1 to 94 $\mu\text{g}/\text{m}^3$, with an average ($\pm 1\sigma$)
281 of $33 \pm 14 \mu\text{g}/\text{m}^3$. Nitrate, sulfate, ammonium and organic aerosol contributed on average 19%, 11%,



282 9% and 58% to total NR-PM₁, which was consistent with the aerosol chemical compositions typically
283 observed in the PRD region featuring organic aerosol as the major constituent of NR-PM₁ and higher

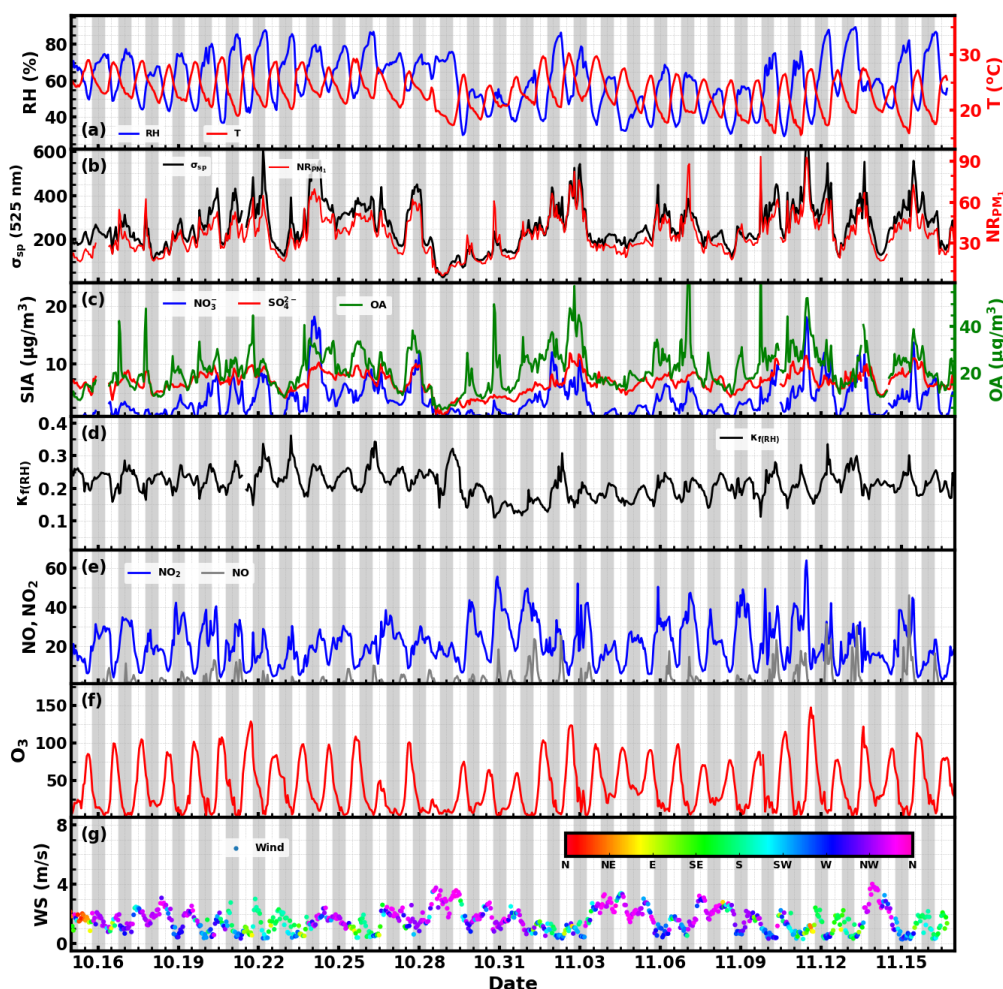


Figure 1. Time series of (a) RH and temperature; (b) aerosol scattering coefficient at 525 nm and mass concentrations of PM₁ non-refractory components; (c) mass concentrations of sulfate, nitrate and organic aerosol; (d) The hygroscopicity parameter κ retrieved from aerosol light scattering enhancement measurements; (e) NO and NO₂ concentrations; (f) O₃ concentration; (g) wind speed/direction. Shaded gray areas corresponding to nighttime periods.

284 sulfate concentration than nitrate concentration (Zhou et al., 2020b). However, the NR-PM₁
285 composition profile differed much from those recently observed in urban Guangzhou (Guo et al., 2020),
286 a megacity about 100 km away from Heshan, where sulfate concentrations were on average only



287 slightly higher than nitrate concentrations during autumn and winter seasons of 2017. The large mass
288 contribution of organic aerosol in PM_{10} resulted in generally moderate ambient aerosol hygroscopicity,
289 with $\kappa_{f(RH)}$ ranging between 0.11 and 0.36 with an average ($\pm 1\sigma$) of 0.22 ± 0.04 . The small standard
290 deviation further suggests for relatively small variations in aerosol hygroscopicity. Sulfate
291 concentrations showed much less daily and diurnal variations than those of nitrate and organic aerosol,
292 suggesting that the sulfate level was determined by the regional scale background, while nitrate and
293 organic aerosol concentration were significantly influenced by local production. Especially, the nitrate
294 concentration usually experienced a sharp increase since sunset and peaks after mid night, sometimes
295 even reached beyond sulfate mass concentration. The time series of NO_2 , NO and O_3 concentration are
296 also shown in Fig.1e and Fig.1f. NO_2 concentration showed distinct diurnal variations, and ranged
297 from 3.5 to 64 ppb with an average ($\pm 1\sigma$) of 20.5 ± 10.5 ppb. The NO concentration ranged from
298 almost 0 to 45 ppb with an average ($\pm 1\sigma$) of 2.2 ± 4.5 ppb, indicating generally low concentrations of
299 NO. O_3 concentrations ranged from 2 to 147 ppb with an average ($\pm 1\sigma$) of 41.5 ± 31.4 ppb, frequently
300 reaching over 90 ppb in the afternoon, indicating for strong daytime photochemistry, and dropped
301 rapidly after sunset towards a very low concentration (usually below 5 ppb) after midnight.

302 The average diurnal variations of NO_2 , NO, O_3 , CO, aerosol chemical compositions, $\kappa_{f(RH)}$ and
303 meteorological parameters are shown in Fig.2. O_3 concentrations began to increase after sunrise,
304 peaked near 15:00 and then began to decrease quickly but drops slower after midnight. Meanwhile,
305 NO concentration began to decrease quickly after sunrise, reached and remained near zero after
306 noontime, and began to slightly increase after 21:00. NO_2 concentration increased quickly after 15:00
307 and reached a plateau after 21:00. Variation characteristics of NO, O_3 , and NO_2 suggest that the
308 relatively low NO concentration resulted in weak titration effects on O_3 , where upon typical NO_3
309 chemistry and subsequent N_2O_5 chemistry was likely to occur, which was likely the mechanism behind
310 the observed nitrate variations. Nitrate concentrations increased quickly since 16:00 and peaked after



311 midnight (about 03:00 LT), further confirming this speculation.

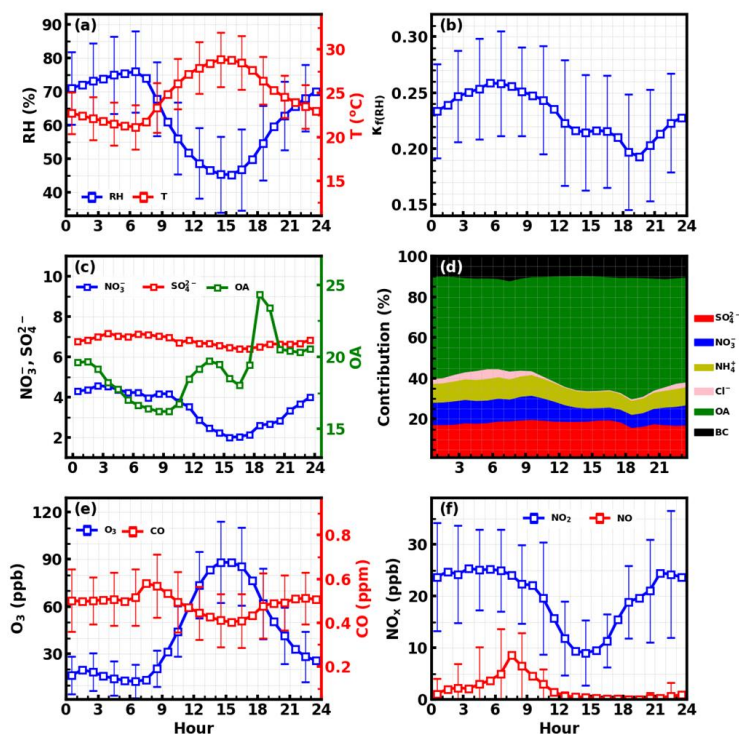


Figure 2. Average diurnal variations of (a) RH and T; (b) $\kappa_{f(RH)}$; (c) sulfate, nitrate and organic aerosol; (d) mass fractions of different components; (e) O_3 and CO; (f) NO_2 and NO.

312 Under the strong daytime photochemistry and nighttime heterogenous formation of nitrate,
313 evident diurnal variations of aerosol hygroscopicity was observed. The overall aerosol hygroscopicity
314 variation was generally consistent with the variation pattern of inorganic aerosol fraction in NR-PM₁
315 as shown in Fig.2d. In detail, the overall variations of nitrate and associated ammonium, as well as
316 organic aerosol determines the general hygroscopicity variation pattern: the quick increase in organic
317 aerosol between 16:00 to 19:00 resulted in the quick $\kappa_{f(RH)}$ decrease during this period; since then
318 the general decrease of organic aerosol and increase of nitrate resulted in the increase of $\kappa_{f(RH)}$ until
319 the next morning; the daytime decrease of nitrate and increase of organic aerosol resulted in a $\kappa_{f(RH)}$
320 decrease before 13:00. Note that sulfate concentration remaining almost constant throughout the day
321 further confirmed previous statement that local production likely contributed less to sulfate



322 concentration, which can be an indicator of regional air mass status.

323 These results suggest that both strong daytime photochemistry and nighttime NO₃ chemistry
324 played significant roles in diurnal variations of organic aerosol and nitrate, while aged regional air
325 mass determined the sulfate concentration, which provides a good opportunity for investigating how
326 typical daytime photochemistry and nighttime NO₃ chemistry and aged regional organic aerosol
327 components impact on organic aerosol hygroscopicity.

328 4.2 κ_{OA} derivations and its relationship with organic aerosol oxidation state

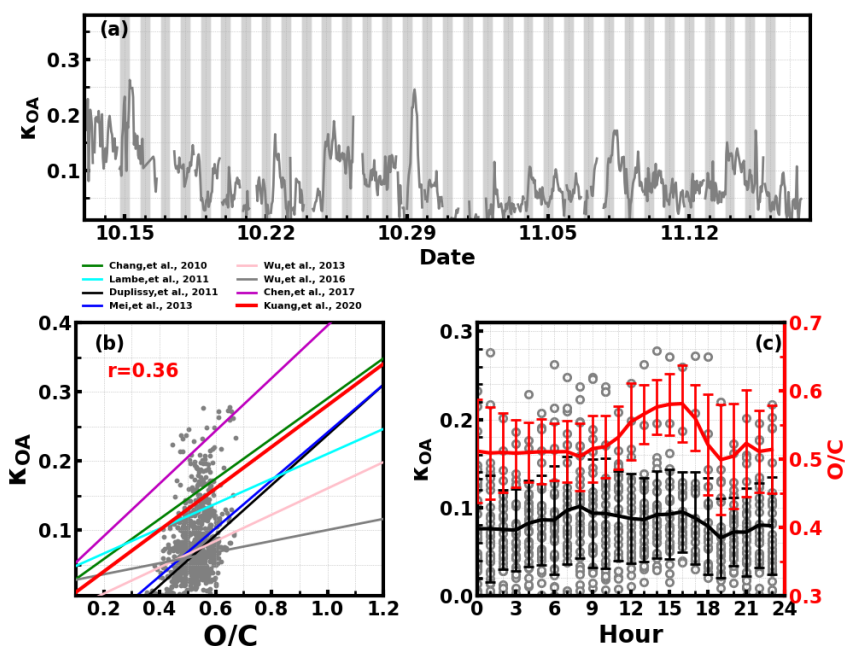


Figure 3. (a) Time series of derived κ_{OA} ; (b) Correlations between O/C ratio and κ_{OA} , lines correspond to empirical relationships between κ_{OA} and O/C ratio reported in different studies; (c) Diurnal variations of κ_{OA} and O/C ratio;

329 The organic aerosol hygroscopicity parameter κ_{OA} was derived according to the method
330 mentioned in Sect.3.2, and the results with hourly time resolution are shown in Fig.3a. κ_{OA} revealed
331 daily and diurnal variations, and ranged from almost zero to 0.28 with an average ($\pm 1\sigma$) of 0.085 ± 0.05 .
332 The relationship between κ_{OA} and O/C was further investigated and shown in Fig.3b. Results



333 demonstrated that κ_{OA} and O/C were weakly correlated during this campaign, with most data points
334 falling in the published κ_{OA} and O/C relationship band. During this campaign, O/C generally resided
335 in a small range (from about 0.4 to 0.6) with an average ($\pm 1\sigma$) of 0.053 ± 0.006 , indicating small
336 variations in O/C, however, featuring drastic variations in κ_{OA} . The average diurnal variations of O/C
337 and κ_{OA} are shown in Fig.3c. On average, κ_{OA} increased slowly during the nighttime and varied
338 even smaller during most of the daytime. Nevertheless, it experienced a relatively quicker decrease
339 from 17:00 to 19:00, which appeared to be coincident with the quick OA concentration increase as
340 shown in Fig.2. However, the O/C increased during the period when O_3 concentration increased
341 quickly, suggesting that daytime photochemistry drove the OA oxidation during daytime. The key
342 point here is that the diurnal patterns of O/C and κ_{OA} differed much from each other, which is why

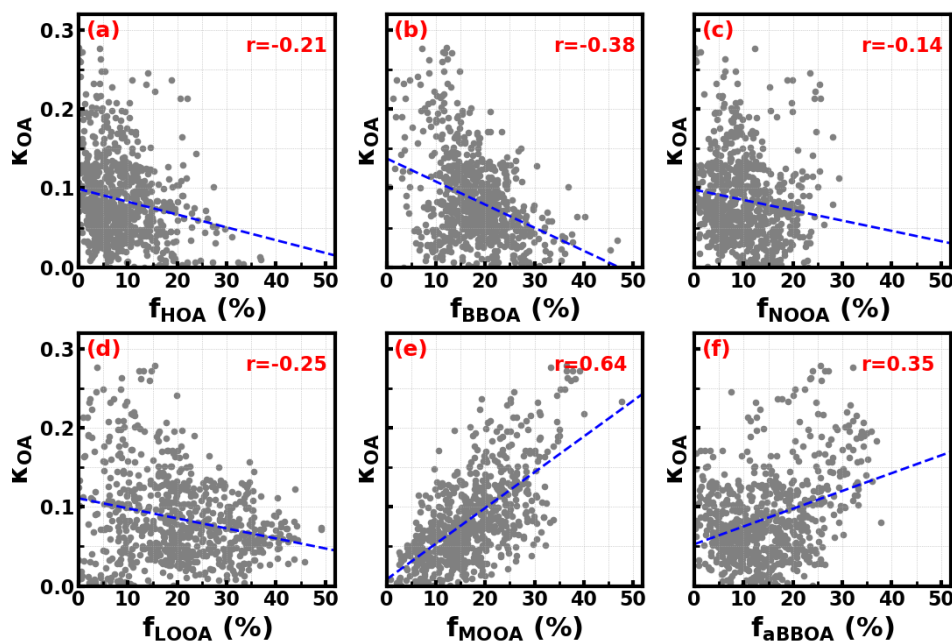


Figure 4. Correlations between κ_{OA} and mass fractions of OA factors in total OA mass.

343 the variation in O/C failed to describe that of κ_{OA} .

344 The question remains which factors were controlling the variations of κ_{OA} . The relationships
345 between κ_{OA} and mass fractions of different PMF OA factors in total OA mass were further
346 investigated and shown in Fig.4. In general, the average ($\pm 1\sigma$) mass fractions of HOA, BBOA, aBBOA,
347 LOOA, Night-OA, and MOOA were: 8.7% ($\pm 7.8\%$), 16.5% ($\pm 8.3\%$), 15.9% ($\pm 10.5\%$), 19.1% (\pm



348 10.9%), 10.4% ($\pm 6.5\%$), 18.6% ($\pm 12.2\%$), and it means that during this campaign SOA dominates
349 organic aerosol (SOA > 70%). Two primary OA factors, HOA and BBOA were related to vehicle
350 exhausts mixed with cooking emissions and to biomass burning emissions, respectively. κ_{OA} was
351 negatively correlated with both HOA and BBOA, which is consistent with previous literature reports
352 that primary OA components such as HOA and BBOA are generally hydrophobic. The average diurnal
353 variations of OA PMF factors shown in Fig.5 demonstrate that both BBOA and HOA peaked near
354 18:00, which should be associated with the frequently observed biomass burning events and supper
355 cooking in villages near the site. This explained the sharp increase of OA mass and the sharp decrease
356 near 18:00 as shown in Fig.3c. It was generally thought that secondary aerosol formation would result

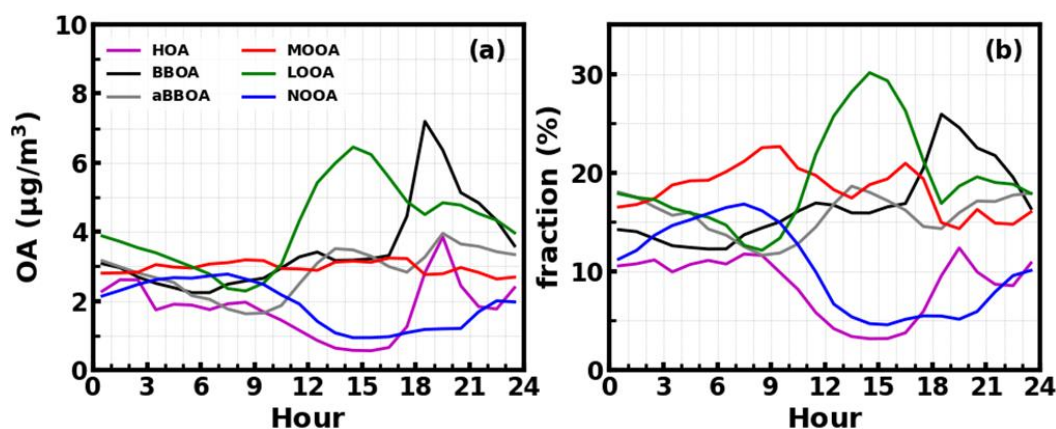


Figure 5. Average diurnal variations of mass concentrations (a) and their mass fractions (b) in total OA mass of different PMF OA factors.

357 in increases of aerosol hygroscopicity. However, κ_{OA} was also negatively correlated with LOOA
358 (Fig.4d), whose mass concentration increase rapidly after sunrise and are likely secondary due to local
359 photochemistry with potential precursors such as isoprene and anthropogenic VOCs. The average O/C
360 ratio for LOOA is 0.72, which is only lower than that of MOOA, suggesting that the daytime OOA
361 formation and decrease of BBOA and HOA mass concentrations drove the increase of daytime O/C,
362 and the negative correlation between κ_{OA} and LOOA mass fraction explained why O/C failed to
363 describe diurnal variations of κ_{OA} . κ_{OA} was also negatively correlated with Night-OA fraction,
364 which increased during nighttime and was highly correlated with nitrate concentrations (Figure S4),
365 which were likely associated the NO_3 nighttime chemistry as discussed in Sect. 4.1. Results of Suda
366 et al. (2014) demonstrated that the addition of NO_3 radical would exert negative impacts on κ_{OA} .



367 which is consistent with the observations shown here. As shown in Fig.4, κ_{OA} was positively
368 correlated with both MOOA and aBBOA, especially with that of MOOA. MOOA was highly
369 correlated with sulfate and showed almost no diurnal variations, indicating that the highly oxygenated
370 (O/C ~1) MOOA was also more associated with regional air masses. The observed small nighttime
371 increase of κ_{OA} could be associated with the slight increase in MOOA mass fraction as shown in
372 Fig.5b. Similar to LOOA, the aBBOA increased during daytime, which revealed quick ageing process
373 of biomass burning related precursors or primary aerosols through photochemistry. Also, the aBBOA
374 factor showed similar variation trend with $C_6H_2NO_4^+$ (m/z 151.998, see Fig. S3) which is a
375 characteristic ion of a typical aged BBOA component nitrocatechol (Bertrand et al., 2018). However,
376 the resolved average O/C ratio of aBBOA was only 0.39, which is even lower than that of BBOA (O/C
377 ~0.48), implying that BBOA were likely formed through oxidation of gaseous BBOA precursors rather
378 than the direct oxidation of BBOA. The fact that nitrocatechol is more likely to be contributed by
379 oxidation of gaseous precursors in biomass burning plumes rather than primary biomass burning
380 emissions (Wang et al., 2019) rationalizes this speculation. The similar diurnal characteristics but
381 contrasting effects of LOOA and aBBOA on κ_{OA} further explains the weak correlation coefficient
382 between κ_{OA} and O/C. However, the weak but positive correlation between κ_{OA} and O/C should
383 have arose from the much stronger positive correlation between κ_{OA} and MOOA mass fractions.
384 LOOA has relatively high O/C and its abundance usually reaches above that of MOOA during the
385 afternoon, however, its negative effects on κ_{OA} was partially compensated by aBBOA which had
386 lower O/C. In addition, κ_{OA} was mostly associated with mass fractions of MOOA with highest O/C,
387 thus giving rise to the weak but positive relationship between κ_{OA} and O/C. As for κ_{OA} diurnal
388 variations, daytime increase of aBBOA and LOOA has compensating effects on κ_{OA} , and the HOA
389 and Night-OA decrease further complicated its variations.

390 4.3 Discussions on complexity of organic aerosol hygroscopicity parameterizations

391 As demonstrated in Sect.4.2, the LOOA factor with higher O/C had negative impacts on κ_{OA} ,
392 while aBBOA with much lower O/C had positive effects on κ_{OA} . These results suggested that O/C is
393 not enough for parameterizing κ_{OA} and the question remains what additional parameters are needed
394 or how should they be implemented? To further explore on this issue, the relationships between κ_{OA}



395 and mass fractions of aBBOA+MOOA in total OA mass ($f_{\text{MOOA+aBBOA}}$) was further investigated to
396 manifest the complexity of κ_{OA} variations and discuss potential impact factors, with results shown in
397 Fig.6a. As discussed in Sect.4.2, both MOOA and aBBOA had positive effects on κ_{OA} , however, the
398 relationship between κ_{OA} and $f_{\text{MOOA+aBBOA}}$ does not yield a higher correlation coefficient than that
399 between κ_{OA} and f_{MOOA} , and the results shown in Fig.6a demonstrate that κ_{OA} and $f_{\text{MOOA+aBBOA}}$
400 might have different relationships during different periods. The relationships between κ_{OA} and
401 $f_{\text{MOOA+aBBOA}}$ during three periods were further investigated and shown in Fig.6b-d, which shows that
402 during the first period from 10-12 to 10-22, κ_{OA} was highly correlated with $f_{\text{MOOA+aBBOA}}$ ($R=0.82$),
403 with all points falling in a narrow band, suggesting that $f_{\text{MOOA+aBBOA}}$ alone could describe the variations
404 in κ_{OA} well. However, during the second period (from 10-23 to 11-02) and the third period (from 11-
405 03 to 11-17) the correlation coefficients between κ_{OA} and $f_{\text{MOOA+aBBOA}}$ were much lower. Obviously,
406 $f_{\text{MOOA+aBBOA}}$ during the second and the third period was in general much lower than that during the
407 first period. The timeseries of κ_{OA} and different PMF OA factors are shown in Fig.7. MOOA
408 displayed relatively small variations during this campaign, highlighting that the regional air mass did
409 not experience tremendous variations, and suggesting that changes of other OA factors especially
410 aBBOA have resulted in different relationships between κ_{OA} and $f_{\text{MOOA+aBBOA}}$. The results in Fig.7c
411 shows that the ratio between aBBOA and BBOA differs much during three periods and declines from
412 the first period to the third period. During the first period, aBBOA was more abundant and was well
413 correlated ($R=0.57$) with BBOA. At the same time, aBBOA was positively correlated with HOA ($R =$
414 0.49) especially with the cooking emission tracer $\text{C}_6\text{H}_{10}\text{O}^+$ ($R = 0.60$), which could be emitted together
415 with biomass burning emissions, when residents in surrounding villages cooked with biomass fuels.
416 BBOA and aBBOA had comparable levels during the second period, however, aBBOA concentration



417 was much lower than that of BBOA during the third period. It can also be noticed that aBBOA in the
418 second period showed higher correlation with BBOA ($R = 0.45$) than that in the last period ($R = 0.17$),
419 which was also the case with cooking emission tracer ($R = 0.60$ for the 2nd period, 0.36 for the 3rd
420 period). These results suggest that the chemical and physical properties of aBBOA likely changed
421 much within the three periods despite similarities in PMF analysis. Both the primary gas pollutants

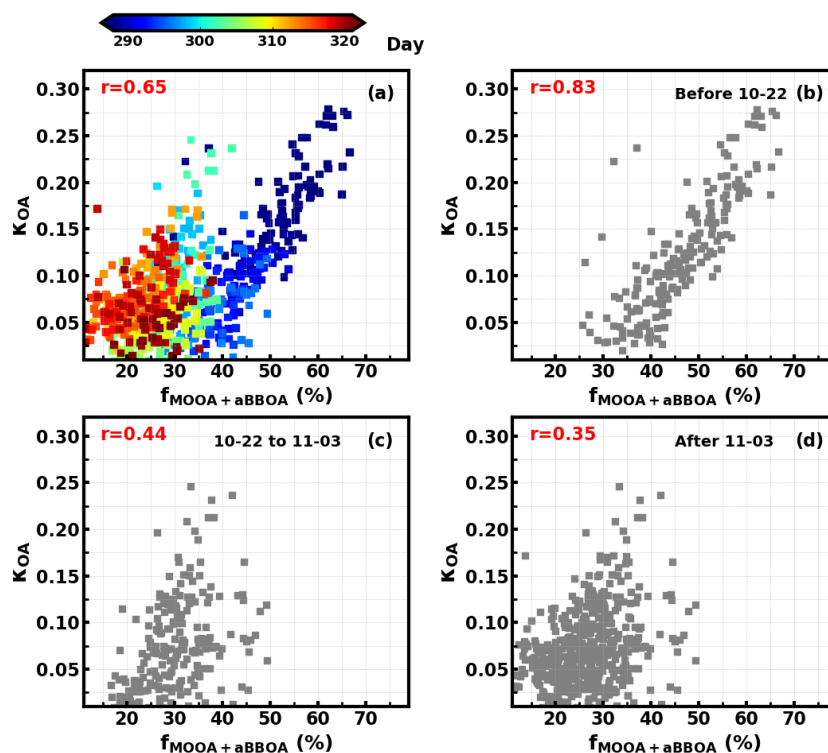


Figure 6. Relationships between κ_{OA} and $f_{MOOA+aBBOA}$ during (a) the entire observation period; (b) 10-12 to 10-22; (c) 10-23 to 11-02; (d) 11-03 to 11-17. Colors of scatter points in (a) represents day of the year.

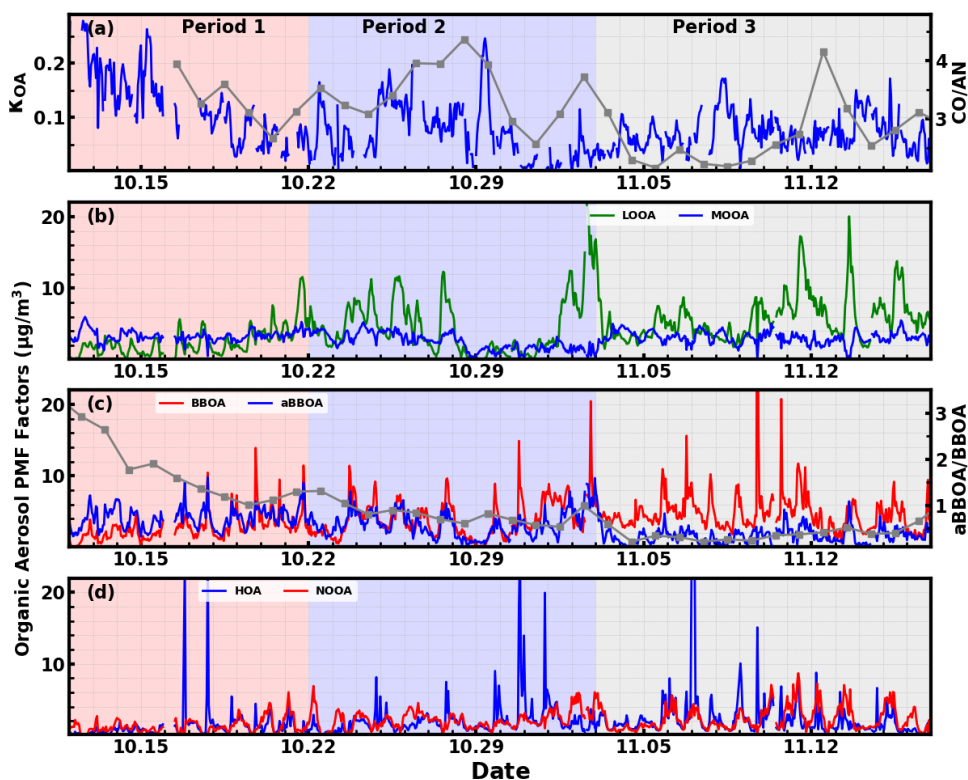


Figure 7. Time series of (a) derived κ_{OA} and the right y-axis represent the ratio between CO and AN (acetonitrile); (b) LOOA and MOOA; (c) BBOA and aged BBOA, and the right axis represents the ratio between aBBOA/BBOA; (d) HOA and NOOA

422 CO and acetonitrile are highly associated with biomass burning and are often used as indicators of
423 biomass burning events, and the ratio between them can somehow indicate the emission profile
424 changes of biomass burning thus the primary VOC profile changes. The time series of the ratio between
425 CO and acetonitrile (Fig.7a) differs much during the three periods, especially for the second and the
426 third period. This difference suggests that although the biomass burning event continued, their
427 emission profiles associated with the burning fuels and conditions likely changed a lot, indicating that
428 aBBOA precursors might have changed during different agricultural activities, thus changing their
429 formation pathways as well as their chemical and physical properties. Other than the aBBOA property
430 changes, changes in OA factor contributions (for example, relative contributions of OA factors other
431 than MOOA and aBBOA) may also impact on the relationship between κ_{OA} and $f_{MOOA+aBBOA}$. Also,
432 the chemical and physical properties of Night-OA and LOOA together with the VOC profile can also



433 have changed.

434 In general, the results shown here deliver the following key messages: (1) Although the O/C failed
435 to describe variations in κ_{OA} , variations of OA factors that are more related to VOC sources or OA
436 formation pathways could sometimes be found to explain the κ_{OA} variations; (2) MOOA, being
437 highly oxygenated and associated with regional air mass, was the most important component that
438 enhanced κ_{OA} , which is consistent with current understandings, i.e., organic aerosol aging processes
439 have significant effects on κ_{OA} . However, the κ_{OA} of secondary organic aerosol does not depend on
440 their O/C (contrary effects of aBBOA and LOOA on κ_{OA}); (3) Organic aerosol hygroscopicity of SOA
441 associated with similar sources might differ much under different conditions (effects of aBBOA on
442 κ_{OA} differ much during different periods). These messages might be instructive to the
443 parameterization of κ_{OA} in the following ways: (1) We might relate κ_{OA} to VOC precursors in
444 laboratory studies, but the laboratory derived empirical relationship will likely fail in application of
445 ambient aerosols due to the formation pathway or the existence of other VOC precursors might result
446 in different chemical properties of ambient formed SOA, such as functional groups, from the laboratory
447 case; (2) It seems more plausible to find parameters other than O/C ratio to parameterize κ_{OA} , which
448 should be independent of sources and associated with the physical properties of OA. Overall, these
449 results further highlighted that κ_{OA} parameterizations can be quite difficult and requires a lot of future
450 efforts.

451 **5 Conclusions**

452 In this study, a field campaign was conducted to characterize κ_{OA} with high time resolution for
453 the first time at a rural site in the PRD region. The observation results showed that both typical NO₃
454 night chemistry (indicated by quick nighttime nitrate formation, extremely low NO concentration and
455 quick nighttime O₃ concentration decrease) and strong daytime photochemical chemistry (indicated
456 by high daytime O₃ concentration) prevailed during this field campaign. SOA dominated OA mass
457 (mass fraction >70% on average), which provided us a unique opportunity to investigate influences of
458 SOA formation on variations in organic aerosol hygroscopicity parameter κ_{OA} . Six OA factors were
459 resolved by the AMS PMF analysis, including two primary OA factors HOA and BBOA and other four
460 secondary OA factors MOOA, LOOA, aBBOA and Night-OA. The results demonstrated that mass
461 increase in both two primary OA factors had negative effects on κ_{OA} , which is consistent with current



462 understandings that POA components have quite low hygroscopicity (usually assumed as hydrophilic),
463 while SOA components had distinct effects on κ_{OA} . MOOA with the highest average O/C of 1 was
464 the most important factor that drives the increase of κ_{OA} , probably related with regional air mass and
465 local production contributes small. However, LOOA with average O/C slightly lower than that of
466 MOOA (O/C \sim 0.72), whose mass concentration increased dramatically during daytime due to local
467 production, had negative effects on κ_{OA} . Surprisingly, aBBOA with similar diurnal patterns to that of
468 LOOA, also formed quickly during daytime, but displayed much lower O/C (0.39), exerting positive
469 effects on κ_{OA} . In addition, κ_{OA} revealed weak negative correlation to Night-OA fraction, which
470 increased during nighttime probably due to the NO₃ nighttime chemistry. This finding is in general
471 consistent with results of Suda et al. (2014) that the addition of NO₃ radical would exert negative
472 impacts on κ_{OA} . As a result, the contrasting effects of LOOA and aBBOA on κ_{OA} resulted in the
473 weak correlation coefficient between κ_{OA} and O/C. κ_{OA} was mostly associated with mass fractions
474 of MOOA with highest O/C although its O/C is only a little higher than that of LOOA, which gave rise
475 to the weak but positive relationship between κ_{OA} and O/C.

476 In general, the results presented in this study demonstrate that the O/C failed to describe variations
477 in κ_{OA} , however, SOA factors with different VOC sources or from different OA formation pathways
478 might have discrepant influences on the κ_{OA} . The contrasting effects of LOOA and aBBOA on κ_{OA}
479 demonstrated that VOC precursors from diverse sources and different SOA formation processes may
480 result in SOA with different chemical composition, functional properties as well as microphysical
481 structure, consequently influencing SOA hygroscopicity. On top of that, the hygroscopicity of SOA
482 associated with similar sources might also differ much during different emission and atmospheric
483 conditions. These results demonstrate that we might relate κ_{OA} to VOC precursors in laboratory
484 studies, but the laboratory derived empirical relationships will likely fail in their application to ambient
485 aerosols due to the more complex formation pathways or the existence of other VOC precursors in the
486 ambient atmosphere, and thus difficult to apply in models. Overall, these results further highlighted
487 that κ_{OA} parameterizations are quite complex, and it is important to conduct more researches on κ_{OA}
488 characterization under different meteorological and source conditions, and examine its relationship
489 with OA and VOC precursor profiles to reach a better characterization and come up with a more
490 appropriate parameterization approach for chemical and climate models.

491



492 **Data availability.** The data used in this study are available from the corresponding author upon request
493 Shan Huang (shanhuang_eci@jnu.edu.cn) and Min Shao (mshao@jnu.edu.cn)

494 **Competing interests.** The authors declare that they have no conflict of interest.

495

496 **Author Contributions.** YK and SH designed the aerosol experiments. YK conceived this research
497 and wrote the manuscript together with SH. YK, BL and BX conducted aerosol light scattering
498 enhancement factor measurements. QS, WC, WL, SH and WH conducted the SP-AMS measurements.
499 MC, YK and SH conducted the particle number size distribution measurements. MS and BY planned
500 this campaign. YP collected and managed criterial pollutants and meteorological parameters from
501 Heshan supersite. PZ provided the humidified nephelometer system and contributed to discussions and
502 revisions of the manuscript. DC and DY provided authority of conducting the campaign in Heshan
503 supersite and gave data availability from the site. All other coauthors have contributed to this paper in
504 different ways.

505

506 **Acknowledgments**

507 This work is supported by the National Natural Science Foundation of China (grant No. 41805109,
508 41807302), National Key Research and Development Program of China (grant No. 2017YFC0212803,
509 2016YFC0202206, 2017YFB0503901), Key-Area Research and Development Program of Guangdong
510 Province (grant No. 2019B110206001), Guangdong Natural Science Foundation (grant No.
511 2018A030313384), Special Fund Project for Science and Technology Innovation Strategy of
512 Guangdong Province (grant No.2019B121205004), Guangdong Natural Science Funds for
513 Distinguished Young Scholar (grant No. 2018B030306037) and Guangdong Innovative and
514 Entrepreneurial Research Team Program (grant No. 2016ZT06N263).

515

516

517

518

519

520



521 References

- 522 Alfarra, M. R., Good, N., Wyche, K. P., Hamilton, J. F., Monks, P. S., Lewis, A. C., and McFiggans, G.: Water uptake is
523 independent of the inferred composition of secondary aerosols derived from multiple biogenic VOCs, *Atmos. Chem. Phys.*,
524 13, 11769-11789, 10.5194/acp-13-11769-2013, 2013.
- 525 Bertrand, A., Stefenelli, G., Jen, C. N., Pieber, S. M., Bruns, E. A., Ni, H., Temime-Roussel, B., Slowik, J. G., Goldstein, A. H.,
526 El Haddad, I., Baltensperger, U., Prévôt, A. S. H., Wortham, H., and Marchand, N.: Evolution of the chemical fingerprint of
527 biomass burning organic aerosol during aging, *Atmos. Chem. Phys.*, 18, 7607-7624, 10.5194/acp-18-7607-2018, 2018.
- 528 Canagaratna, M. R., Jayne, J. T., Jimenez, J. L., Allan, J. D., Alfarra, M. R., Zhang, Q., Onasch, T. B., Drewnick, F., Coe, H.,
529 Middlebrook, A., Delia, A., Williams, L. R., Trimborn, A. M., Northway, M. J., DeCarlo, P. F., Kolb, C. E., Davidovits, P., and
530 Worsnop, D. R.: Chemical and microphysical characterization of ambient aerosols with the aerodyne aerosol mass
531 spectrometer, *Mass Spectrom. Rev.*, 26, 185-222, 10.1002/mas.20115, 2007.
- 532 Cerully, K. M., Bougiatioti, A., Hite Jr, J. R., Guo, H., Xu, L., Ng, N. L., Weber, R., and Nenes, A.: On the link between
533 hygroscopicity, volatility, and oxidation state of ambient and water-soluble aerosols in the southeastern United States,
534 *Atmos. Chem. Phys.*, 15, 8679-8694, 10.5194/acp-15-8679-2015, 2015.
- 535 Chen, J., Zhao, C. S., Ma, N., and Yan, P.: Aerosol hygroscopicity parameter derived from the light scattering enhancement
536 factor measurements in the North China Plain, *Atmos. Chem. Phys. Discuss.*, 14, 3459-3497, 10.5194/acpd-14-3459-2014,
537 2014.
- 538 Deng, Y., Yai, H., Fujinari, H., Kawana, K., Nakayama, T., and Mochida, M.: Diurnal variation and size dependence of the
539 hygroscopicity of organic aerosol at a forest site in Wakayama, Japan: their relationship to CCN concentrations, *Atmos.*
540 *Chem. Phys.*, 19, 5889-5903, 10.5194/acp-19-5889-2019, 2019.
- 541 Gunthe, S. S., Rose, D., Su, H., Garland, R. M., Achtert, P., Nowak, A., Wiedensohler, A., Kuwata, M., Takegawa, N., Kondo,
542 Y., Hu, M., Shao, M., Zhu, T., Andreae, M. O., and Pöschl, U.: Cloud condensation nuclei (CCN) from fresh and aged air
543 pollution in the megacity region of Beijing, *Atmos. Chem. Phys.*, 11, 11023-11039, 10.5194/acp-11-11023-2011, 2011.
- 544 Guo, J., Zhou, S., Cai, M., Zhao, J., Song, W., Zhao, W., Hu, W., Sun, Y., He, Y., Yang, C., Xu, X., Zhang, Z., Cheng, P., Fan, Q.,
545 Hang, J., Fan, S., Wang, X., and Wang, X.: Characterization of submicron particles by time-of-flight aerosol chemical
546 speciation monitor (ToF-ACSM) during wintertime: aerosol composition, sources, and chemical processes in Guangzhou,
547 China, *Atmospheric Chemistry and Physics*, 20, 7595-7615, 10.5194/acp-20-7595-2020, 2020.
- 548 Gysel, M., Crosier, J., Topping, D. O., Whitehead, J. D., Bower, K. N., Cubison, M. J., Williams, P. I., Flynn, M. J., McFiggans,
549 G. B., and Coe, H.: Closure study between chemical composition and hygroscopic growth of aerosol particles during
550 TORCH2, *Atmos. Chem. Phys.*, 7, 6131-6144, 10.5194/acp-7-6131-2007, 2007.
- 551 Hong, J., Xu, H., Tan, H., Yin, C., Hao, L., Li, F., Cai, M., Deng, X., Wang, N., Su, H., Cheng, Y., Wang, L., Petäjä, T., and
552 Kerminen, V. M.: Mixing state and particle hygroscopicity of organic-dominated aerosols over the Pearl River Delta region
553 in China, *Atmos. Chem. Phys.*, 18, 14079-14094, 10.5194/acp-18-14079-2018, 2018.
- 554 Jimenez, J. L., Canagaratna, M. R., Donahue, N. M., Prevot, A. S. H., Zhang, Q., Kroll, J. H., DeCarlo, P. F., Allan, J. D., Coe,
555 H., Ng, N. L., Aiken, A. C., Docherty, K. S., Ulbrich, I. M., Grieshop, A. P., Robinson, A. L., Duplissy, J., Smith, J. D., Wilson, K.
556 R., Lanz, V. A., Hueglin, C., Sun, Y. L., Tian, J., Laaksonen, A., Raatikainen, T., Rautiainen, J., Vaattovaara, P., Ehn, M., Kulmala,
557 M., Tomlinson, J. M., Collins, D. R., Cubison, M. J., Dunlea, J., Huffman, J. A., Onasch, T. B., Alfarra, M. R., Williams, P. I.,
558 Bower, K., Kondo, Y., Schneider, J., Drewnick, F., Borrmann, S., Weimer, S., Demerjian, K., Salcedo, D., Cottrell, L., Griffin,



- 559 R., Takami, A., Miyoshi, T., Hatakeyama, S., Shimono, A., Sun, J. Y., Zhang, Y. M., Dzepina, K., Kimmel, J. R., Sueper, D., Jayne,
560 J. T., Herndon, S. C., Trimborn, A. M., Williams, L. R., Wood, E. C., Middlebrook, A. M., Kolb, C. E., Baltensperger, U., and
561 Worsnop, D. R.: Evolution of Organic Aerosols in the Atmosphere, *Science*, 326, 1525-1529, 10.1126/science.1180353,
562 2009.
- 563 Jin, X., Wang, Y., Li, Z., Zhang, F., Xu, W., Sun, Y., Fan, X., Chen, G., Wu, H., Ren, J., Wang, Q., and Cribb, M.: Significant
564 contribution of organics to aerosol liquid water content in winter in Beijing, China, *Atmos. Chem. Phys.*, 20, 901-914,
565 10.5194/acp-20-901-2020, 2020.
- 566 Jing, B., Wang, Z., Tan, F., Guo, Y., Tong, S., Wang, W., Zhang, Y., and Ge, M.: Hygroscopic behavior of atmospheric aerosols
567 containing nitrate salts and water-soluble organic acids, *Atmospheric Chemistry and Physics*, 18, 5115-5127, 10.5194/acp-
568 18-5115-2018, 2018.
- 569 Koehler, K. A., Kreidenweis, S. M., DeMott, P. J., Petters, M. D., Prenni, A. J., and Carrico, C. M.: Hygroscopicity and cloud
570 droplet activation of mineral dust aerosol, *Geophysical Research Letters*, 36, 10.1029/2009GL037348, 2009.
- 571 Kuang, Y., Zhao, C., Tao, J., Bian, Y., Ma, N., and Zhao, G.: A novel method for deriving the aerosol hygroscopicity parameter
572 based only on measurements from a humidified nephelometer system, *Atmos. Chem. Phys.*, 17, 6651-6662, 10.5194/acp-
573 17-6651-2017, 2017.
- 574 Kuang, Y., He, Y., Xu, W., Zhao, P., Cheng, Y., Zhao, G., Tao, J., Ma, N., Su, H., Zhang, Y., Sun, J., Cheng, P., Yang, W., Zhang,
575 S., Wu, C., Sun, Y., and Zhao, C.: Distinct diurnal variation in organic aerosol hygroscopicity and its relationship with
576 oxygenated organic aerosol, *Atmos. Chem. Phys.*, 20, 865-880, 10.5194/acp-20-865-2020, 2020a.
- 577 Kuang, Y., Xu, W., Tao, J., Ma, N., Zhao, C., and Shao, M.: A Review on Laboratory Studies and Field Measurements of
578 Atmospheric Organic Aerosol Hygroscopicity and Its Parameterization Based on Oxidation Levels, *Current Pollution*
579 *Reports*, 10.1007/s40726-020-00164-2, 2020b.
- 580 Kuwata, M., Zorn, S. R., and Martin, S. T.: Using Elemental Ratios to Predict the Density of Organic Material Composed of
581 Carbon, Hydrogen, and Oxygen, *Environmental science & technology*, 46, 787-794, 10.1021/es202525q, 2012.
- 582 Lambe, A. T., Onasch, T. B., Massoli, P., Croasdale, D. R., Wright, J. P., Ahern, A. T., Williams, L. R., Worsnop, D. R., Brune,
583 W. H., and Davidovits, P.: Laboratory studies of the chemical composition and cloud condensation nuclei (CCN) activity of
584 secondary organic aerosol (SOA) and oxidized primary organic aerosol (OPOA), *Atmos. Chem. Phys.*, 11, 8913-8928,
585 10.5194/acp-11-8913-2011, 2011.
- 586 Latham, T. L., Beyersdorf, A. J., Thornhill, K. L., Winstead, E. L., Cubison, M. J., Hecobian, A., Jimenez, J. L., Weber, R. J.,
587 Anderson, B. E., and Nenes, A.: Analysis of CCN activity of Arctic aerosol and Canadian biomass burning during summer
588 2008, *Atmos. Chem. Phys.*, 13, 2735-2756, 10.5194/acp-13-2735-2013, 2013.
- 589 Li, X., Song, S., Zhou, W., Hao, J., Worsnop, D. R., and Jiang, J.: Interactions between aerosol organic components and liquid
590 water content during haze episodes in Beijing, *Atmos. Chem. Phys.*, 19, 12163-12174, 10.5194/acp-19-12163-2019, 2019.
- 591 Liu, H. J., Zhao, C. S., Nekat, B., Ma, N., Wiedensohler, A., van Pinxteren, D., Spindler, G., Müller, K., and Herrmann, H.:
592 Aerosol hygroscopicity derived from size-segregated chemical composition and its parameterization in the North China
593 Plain, *Atmos. Chem. Phys.*, 14, 2525-2539, 10.5194/acp-14-2525-2014, 2014.
- 594 Liu, P., Song, M., Zhao, T., Gunthe, S. S., Ham, S., He, Y., Qin, Y. M., Gong, Z., Amorim, J. C., Bertram, A. K., and Martin, S.
595 T.: Resolving the mechanisms of hygroscopic growth and cloud condensation nuclei activity for organic particulate matter,
596 *Nature communications*, 9, 4076, 10.1038/s41467-018-06622-2, 2018.



- 597 Liu, X., and Wang, J.: How important is organic aerosol hygroscopicity to aerosol indirect forcing?, *Environmental Research*
598 *Letters*, 5, 044010, 10.1088/1748-9326/5/4/044010, 2010.
- 599 Luo, Q., Hong, J., Xu, H., Han, S., Tan, H., Wang, Q., Tao, J., Ma, N., Cheng, Y., and Su, H.: Hygroscopicity of amino acids and
600 their effect on the water uptake of ammonium sulfate in the mixed aerosol particles, *The Science of the total environment*,
601 734, 139318, 10.1016/j.scitotenv.2020.139318, 2020.
- 602 Marsh, A., Miles, R. E. H., Rovelli, G., Cowling, A. G., Nandy, L., Dutcher, C. S., and Reid, J. P.: Influence of organic compound
603 functionality on aerosol hygroscopicity: dicarboxylic acids, alkyl-substituents, sugars and amino acids, *Atmospheric*
604 *Chemistry and Physics*, 17, 5583-5599, 10.5194/acp-17-5583-2017, 2017.
- 605 Massoli, P., Lambe, A. T., Ahern, A. T., Williams, L. R., Ehn, M., Mikkilä, J., Canagaratna, M. R., Brune, W. H., Onasch, T. B.,
606 Jayne, J. T., Petäjä, T., Kulmala, M., Laaksonen, A., Kolb, C. E., Davidovits, P., and Worsnop, D. R.: Relationship between
607 aerosol oxidation level and hygroscopic properties of laboratory generated secondary organic aerosol (SOA) particles,
608 *Geophysical Research Letters*, 37, 10.1029/2010gl045258, 2010.
- 609 Middlebrook, A. M., Bahreini, R., Jimenez, J. L., and Canagaratna, M. R.: Evaluation of Composition-Dependent Collection
610 Efficiencies for the Aerodyne Aerosol Mass Spectrometer using Field Data, *Aerosol Science and Technology*, 46, 258-271,
611 10.1080/02786826.2011.620041, 2012.
- 612 Onasch, T. B., Trimborn, A., Fortner, E. C., Jayne, J. T., Kok, G. L., Williams, L. R., Davidovits, P., and Worsnop, D. R.: Soot
613 Particle Aerosol Mass Spectrometer: Development, Validation, and Initial Application, *Aerosol Sci. Tech.*, 46, 804-817,
614 10.1080/02786826.2012.663948, 2012.
- 615 Paatero, P., and Tapper, U.: Positive matrix factorization: A non-negative factor model with optimal utilization of error
616 estimates of data values, *Environmetrics*, 5, 111-126, 10.1002/env.3170050203, 1994.
- 617 Paatero, P.: Least squares formulation of robust non-negative factor analysis, *Chemometr Intell Lab*, 37, 23-35,
618 10.1016/S0169-7439(96)00044-5, 1997.
- 619 Peng, C., Gu, W., Li, R., Lin, Q., Ma, Q., Jia, S., Krishnan, P., Wang, X., and Tang, M.: Large Variations in Hygroscopic
620 Properties of Unconventional Mineral Dust, *ACS Earth and Space Chemistry*, 4, 1823-1830,
621 10.1021/acsearthspacechem.0c00219, 2020.
- 622 Petters, M. D., and Kreidenweis, S. M.: A single parameter representation of hygroscopic growth and cloud condensation
623 nucleus activity, *Atmospheric Chemistry and Physics*, 7, 1961-1971, 2007.
- 624 Petters, S. S., Pagonis, D., Clafflin, M. S., Levin, E. J. T., Petters, M. D., Ziemann, P. J., and Kreidenweis, S. M.: Hygroscopicity
625 of Organic Compounds as a Function of Carbon Chain Length and Carboxyl, Hydroperoxy, and Carbonyl Functional Groups,
626 *The Journal of Physical Chemistry A*, 121, 5164-5174, 10.1021/acs.jpca.7b04114, 2017.
- 627 Rastak, N., Pajunoja, A., Acosta Navarro, J. C., Ma, J., Song, M., Partridge, D. G., Kirkevåg, A., Leong, Y., Hu, W. W., Taylor,
628 N. F., Lambe, A., Cerully, K., Bougiatioti, A., Liu, P., Krejci, R., Petäjä, T., Percival, C., Davidovits, P., Worsnop, D. R., Ekman,
629 A. M. L., Nenes, A., Martin, S., Jimenez, J. L., Collins, D. R., Topping, D. O., Bertram, A. K., Zuend, A., Virtanen, A., and
630 Riipinen, I.: Microphysical explanation of the RH-dependent water affinity of biogenic organic aerosol and its importance
631 for climate, *Geophysical Research Letters*, 44, 5167-5177, 10.1002/2017gl073056, 2017.
- 632 Rickards, A. M. J., Miles, R. E. H., Davies, J. F., Marshall, F. H., and Reid, J. P.: Measurements of the Sensitivity of Aerosol
633 Hygroscopicity and the κ Parameter to the O/C Ratio, *The Journal of Physical Chemistry A*, 117, 14120-14131,
634 10.1021/jp407991n, 2013.



- 635 Suda, S. R., Petters, M. D., Yeh, G. K., Strollo, C., Matsunaga, A., Faulhaber, A., Ziemann, P. J., Prenni, A. J., Carrico, C. M.,
636 Sullivan, R. C., and Kreidenweis, S. M.: Influence of Functional Groups on Organic Aerosol Cloud Condensation Nucleus
637 Activity, *Environmental science & technology*, 48, 10182-10190, 10.1021/es502147y, 2014.
- 638 Ulbrich, I. M., Canagaratna, M. R., Zhang, Q., Worsnop, D. R., and Jimenez, J. L.: Interpretation of organic components
639 from Positive Matrix Factorization of aerosol mass spectrometric data, *Atmos. Chem. Phys.*, 9, 2891-2918, 10.5194/acp-
640 9-2891-2009, 2009.
- 641 Wang, Y., Hu, M., Wang, Y., Zheng, J., Shang, D., Yang, Y., Liu, Y., Li, X., Tang, R., Zhu, W., Du, Z., Wu, Y., Guo, S., Wu, Z., Lou,
642 S., Hallquist, M., and Yu, J. Z.: The formation of nitro-aromatic compounds under high NO_x and anthropogenic VOC
643 conditions in urban Beijing, China, *Atmos. Chem. Phys.*, 19, 7649-7665, 10.5194/acp-19-7649-2019, 2019.
- 644 Wu, Z. J., Poulain, L., Henning, S., Dieckmann, K., Birmili, W., Merkel, M., van Pinxteren, D., Spindler, G., Müller, K.,
645 Stratmann, F., Herrmann, H., and Wiedensohler, A.: Relating particle hygroscopicity and CCN activity to chemical
646 composition during the HCCT-2010 field campaign, *Atmos. Chem. Phys.*, 13, 7983-7996, 10.5194/acp-13-7983-2013, 2013.
- 647 Wu, Z. J., Zheng, J., Shang, D. J., Du, Z. F., Wu, Y. S., Zeng, L. M., Wiedensohler, A., and Hu, M.: Particle hygroscopicity and
648 its link to chemical composition in the urban atmosphere of Beijing, China, during summertime, *Atmos. Chem. Phys.*, 16,
649 1123-1138, 10.5194/acp-16-1123-2016, 2016.
- 650 Xu, W., Kuang, Y., Bian, Y., Liu, L., Li, F., Wang, Y., Xue, B., Luo, B., Huang, S., Yuan, B., Zhao, P., and Shao, M.: Current
651 Challenges in Visibility Improvement in Southern China, *Environmental Science & Technology Letters*, 7, 395-401,
652 10.1021/acs.estlett.0c00274, 2020.
- 653 Yeung, M. C., Lee, B. P., Li, Y. J., and Chan, C. K.: Simultaneous HTDMA and HR-ToF-AMS measurements at the HKUST
654 Supersite in Hong Kong in 2011, *Journal of Geophysical Research: Atmospheres*, 119, 9864-9883, 10.1002/2013JD021146,
655 2014.
- 656 Zhao, D. F., Buchholz, A., Kortner, B., Schlag, P., Rubach, F., Fuchs, H., Kiendler-Scharr, A., Tillmann, R., Wahner, A., Watne,
657 Å. K., Hallquist, M., Flores, J. M., Rudich, Y., Kristensen, K., Hansen, A. M. K., Glasius, M., Kourtchev, I., Kalberer, M., and
658 Mentel, T. F.: Cloud condensation nuclei activity, droplet growth kinetics, and hygroscopicity of biogenic and
659 anthropogenic secondary organic aerosol (SOA), *Atmospheric Chemistry and Physics*, 16, 1105-1121, 10.5194/acp-16-
660 1105-2016, 2016.
- 661 Zhou, W., Xu, W., Kim, H., Zhang, Q., Fu, P., Worsnop, D. R., and Sun, Y.: A review of aerosol chemistry in Asia: insights from
662 aerosol mass spectrometer measurements, *Environmental Science: Processes & Impacts*, 10.1039/D0EM00212G, 2020a.
- 663 Zhou, W., Xu, W., Kim, H., Zhang, Q., Fu, P., Worsnop, D. R., and Sun, Y.: A review of aerosol chemistry in Asia: insights from
664 aerosol mass spectrometer measurements, *Environmental Science: Processes & Impacts*, 22, 1616-1653,
665 10.1039/D0EM00212G, 2020b.
- 666
667
668